

# Autonomous Low Earth Orbit Station-Keeping with Electric Propulsion

Andrea Garulli<sup>1</sup>, Antonio Giannitrapani<sup>2</sup>  
*Università degli Studi di Siena, Siena, 53100, Italy*

Mirko Leomanni<sup>3</sup>, Fabrizio Scortecci<sup>4</sup>  
*Aerospazio Tecnologie s.r.l., Rapolano Terme, 53040, Siena, Italy*

This paper studies the application of an electric propulsion system for autonomous station-keeping of a remote sensing spacecraft flying at low altitude. The considered propulsion system exploits a Xenon propellant bus, which operates both a low power Hall effect thruster and a resistojet. The former is used for continuous in-track control, while the latter provides the impulsive thrusts necessary for cross-track maneuvers. The adopted navigation solution is based on an extended Kalman filter, employing gyro, star-tracker and GPS measurements. Lyapunov-based and proportional-derivative feedback laws are used for orbit and attitude control, respectively. The performance of the proposed electric propulsion system and guidance, navigation and control solution is evaluated on a low Earth orbit mission.

---

<sup>1</sup> Professor, Dipartimento di Ingegneria dell'Informazione (DII) , garulli@ing.unisi.it.

<sup>2</sup> Assistant Professor, Dipartimento di Ingegneria dell'Informazione (DII) , giannitrapani@ing.unisi.it.

<sup>3</sup> Research Engineer, Aerospazio Tecnologie s.r.l., leomanni@libero.it.

<sup>4</sup> Chairman, Aerospazio Tecnologie s.r.l., fscortecci@aerospazio.com.

## Nomenclature

$\mathbf{a}$	= Spacecraft acceleration, $\text{m/s}^2$
$a$	= Semi-major axis, m
$\mathbf{e}$	= Mean orbital elements vector
$e$	= Orbit eccentricity
$e_x$	= Eccentricity vector x-component
$e_y$	= Eccentricity vector y-component
$f$	= Scale factor bias, ppm
$g$	= Standard gravity, $\text{m/s}^2$
$\mathbf{I}$	= Inertia matrix
$I$	= Specific impulse, s
$i$	= Orbit inclination, rad
$M$	= Mean anomaly, rad
$m$	= Spacecraft mass, kg
$\mathbf{p}$	= Thrust, N
$\mathbf{q}_{IB}$	= Quaternion, Inertial $\rightarrow$ Body frame
$\mathbf{q}(\mathbf{R})$	= Quaternion from a rotation matrix $\mathbf{R}$
$\mathbf{R}_{IE}$	= Rotation matrix, Inertial $\rightarrow$ ECEF frame
$\mathbf{R}_{IF}$	= Rotation matrix, Inertial $\rightarrow$ Frenet frame
$\mathbf{R}(\mathbf{q})$	= Rotation matrix from a quaternion $\mathbf{q}$
$\mathbf{r}$	= Spacecraft position, m
$u$	= Spacecraft mean argument of latitude, rad
$\mathbf{v}$	= Spacecraft velocity, $\text{m/s}$
$\Delta\mathbf{v}$	= Impulsive delta-v, $\text{m/s}$
$\delta$	= Error operator, $\delta\mathbf{x} = \mathbf{x} - \hat{\mathbf{x}}$ and $\delta\bar{\mathbf{x}} = \bar{\mathbf{x}} - \hat{\mathbf{x}}$
$\delta\mathbf{q}(\cdot)$	= Quaternion from a small rotation
$\delta(t-t')$	= Dirac delta function, $\text{s}^{-1}$
$\delta_{k\ k'}$	= Kronecker delta function

$\epsilon$  = Alignment error, rad

$\theta$  = Rotation vector for attitude error, rad

$\mu$  = Earth gravitational parameter,  $\text{m}^3/\text{s}^2$

$\tau$  = Spacecraft torque, Nm

$\omega$  = Argument of perigee, rad

$\omega$  = Spacecraft angular velocity, rad/s

$\Omega$  = Right ascension of the ascending node, rad

### *Subscripts*

$c$  = Commanded value

$d$  = Atmospheric drag perturbation

$e$  = SRP, magnetic and lunisolar perturbations

$g$  = Gravitational perturbation

$J2$  = J2 gravity perturbation

$o$  = Osculating elements

$u$  = Control input

### *Superscripts*

$B$  = Vector expressed in the body frame

$E$  = Vector expressed in the ECEF frame

$F$  = Vector expressed in the Frenet frame

$*$  = Quaternion conjugate

$-$  = Time instant before update step

$+$  = Time instant after update step

$\downarrow$  = Time instant before an impulsive burn

$\uparrow$  = Time instant after an impulsive burn

### *Accents*

$\vee$  = Measured values

$\wedge$  = Estimated values

$\sim$  = Measurement residuals

$-$  = Reference values

### *Other symbols*

$\mathbf{0}_{j \times k}$  = Zero matrix with  $j$  rows and  $k$  columns

$\mathbf{I}_{j \times k}$  = Identity matrix with  $j$  rows and  $k$  columns

$\circ$  = Quaternion product

$[\boldsymbol{\omega} \times]$  = Skew-symmetric matrix from vector  $\boldsymbol{\omega}$

## **I. Introduction**

Electric propulsion (EP) represents nowadays a solid established technology which can provide benefits over large number of spacecraft missions and enable new class of challenging applications. This is mainly due to the intrinsic nature of the EP technology, which optimizes the high specific impulse performance accepting low thrust values in return. While the use of such technology on commercial geostationary satellites and deep space missions are widely discussed in the literature (e.g. [1–5]), relatively few studies have been proposed for low Earth orbit (LEO) missions. Nevertheless, the EP capability of providing continuous thrust over several thousands of hours, together with the reduced propellant mass consumption, allows for accurate LEO station-keeping operations over sufficiently long duration missions. In this regard, the GOCE mission represents a breakthrough in space technology [6, 7]. Some recent studies have been focused on drag free spacecraft operations [8, 9]. Besides these challenging scientific missions, there are other classes of LEO missions that have a potential commercial interest, like Earth observation by means of small and cheap satellites. In [10] it is shown that high resolution imagery can be achieved, by using reduced-size optical mapping instruments, from altitudes of about 300 km and below.

Maintaining a given low Earth orbit traditionally requires frequent, ground-based control actions, in order to compensate for atmospheric drag and other perturbative forces. For small, low

cost satellites, ground-in-the-loop control can be a dominant element of both cost and risk [11]. In addition, it is typically based on impulsive control schemes, which are strongly penalized by the large amount of delta-v needed for drag compensation, thus resulting in a limited satellite lifetime. The combined use of new low power EP technologies and autonomous GNC techniques provides an effective way to address these issues. In particular, the use of a suitable electric propulsion system allows for significant savings on propellant mass and a consequent increase of the spacecraft lifetime. On the other hand, autonomous station-keeping provides reduced spacecraft operation costs. The proposed combination of technologies enables a vast number of future low-budget observation missions, which could find a mass-market e.g. in cartographic applications.

In this work, we investigate the application of an electric propulsion system for autonomous station-keeping of a given low Earth orbit, performed by a 100 kg observation minisatellite that carries an electro-optical payload. The EP system is based on the same Xenon propellant bus, which operates a low power Hall effect thruster and a resistojet. The former features a high specific impulse and provides continuous low thrust in the tangential direction, while the latter generates a higher thrust level to perform out-of-plane impulsive maneuvers. This results in a hybrid continuous/impulsive control scheme. Attitude stabilization is addressed using three momentum wheels. The control system is required to keep the spacecraft orbit within a maximum absolute distance of 400 m from a 228 km sun-synchronous, repeat-groundtrack and frozen reference orbit, while the required attitude control accuracy is  $0.2^\circ$ . In order to meet these specifications, a suitable GNC system is presented. The navigation solution is based on an extended Kalman filter that estimates position and attitude of the spacecraft from the available gyro, star-tracker and GPS measurements. A control law based on the Gauss variational equations (GVEs), suitably modified to account for the proposed thruster configuration and the large amount of atmospheric drag acting on the satellite, is used for orbit control, while a proportional-derivative feedback law is employed for attitude control. The reference mission has been simulated in order to validate the proposed GNC solution and to evaluate the performance of the hybrid propulsion system, in terms of achievable accuracy, Hall thruster and resistojet operating regime and propellant mass consumption. An estimate of the mission expected lifetime, considering a given propellant mass fraction of 0.12, is found to be

approximately 200 days.

The paper is organized as follows. In Section II, the reference mission considered in the paper is described, in terms of desired orbit and navigation requirements. In Section III, the dynamic model adopted for the spacecraft is presented, together with a description of the sensor and actuator characteristics. In Section IV, the guidance, navigation and control system developed for the proposed mission is illustrated. In Section V, results of numerical simulations are reported. In Section VI, some conclusions are drawn and future directions of research are outlined.

## II. Reference mission

The objective of the reference mission is to maintain the nominal orbit and attitude of a small remote sensing satellite, with given accuracy and lifetime requirements, through a suitable autonomous GNC technique. In the following, details of the mission, navigation requirements, and spacecraft configuration, are provided.

### A. Orbit and attitude

The reference mission orbit is a specialized sun-synchronous, repeat ground-track and frozen orbit, which is a common design for low Earth observation satellites [12]. The orbit is nearly circular, with an altitude of around 228 km, which corresponds to a 5 day ground-track repeat period. The initial orbital elements are derived by using a simplified J2 and J3 zonal harmonics analysis and refined through numerical simulations, ignoring all the periodic orbital perturbations [13]. Since the orbit is nearly circular, the eccentricity vector and mean argument of latitude replace the eccentricity, argument of perigee and mean anomaly. Table 1 shows the initial nominal values of the mean orbital elements for the chosen reference mission.

The reference orbit is defined in such a way that gravitational perturbations, which cause the sun synchronous secular motion of  $\dot{\Omega} = 360^\circ/\text{year}$ , do not need to be counteracted. As a consequence, the propulsion system is activated only to compensate for non gravitational disturbances, by means of orbital elements control [14]. The dominant non gravitational perturbing forces on the reference orbit are due to atmospheric drag and resonance effects induced by the Sun. The most significant effects of these perturbations on the orbital elements are a constant decay in the semi-major axis,

**Table 1 Orbital elements (initial nominal values)**

Semi-major axis	$a$	6591.338 km
Inclination	$i$	96.3862°
Eccentricity vector x-component	$e_x = e \cos \omega$	0
Eccentricity vector y-component	$e_y = e \sin \omega$	0.0011
Right ascension of the ascending node	$\Omega$	10°
Mean argument of latitude	$u = M + \omega$	270° + 90° = 0°

in the order of 300 m per revolution, and a minor secular inclination drift.

The spacecraft is nominally aligned with a Frenet frame along the orbit. This is a rotating frame centered at the satellite center of mass, and therefore it is not inertial. In this work, the  $X$  axis is always tangential to the orbit, aligned to the velocity vector of the spacecraft. The  $Y$  axis is normal to the orbital plane, being parallel with the angular momentum vector ( $\mathbf{h} = \mathbf{r} \times \mathbf{v}$ ). The  $Z$  axis completes the reference frame ( $Z = X \times Y$ ) and it is always aligned with the position vector for circular orbits. The  $X$ ,  $Y$  and  $Z$  axes define the in-track, cross-track and normal directions. The in-track and normal directions are approximately aligned to the along-track and radial directions of a local vertical/local horizontal (LVLH) frame for nearly circular orbits.

## B. Navigation and control requirements

On-board sensors and actuators are selected in order to meet the navigation and control accuracy requirements, considering the constraints imposed by the spacecraft size. The driving requirement for orbit control is to keep the satellite orbit within a maximum distance of 400 m from the reference orbit. Based on this limitation, a preliminary estimate of the required navigation system accuracy of about 40 m may be considered. Hence, for absolute position determination purposes, it is sufficient to consider a GPS navigation solution in a loosely-coupled GPS/INS integration scheme, capable of providing positioning accuracy of about 20 m. Attitude determination is carried out using star-tracker and three-axis gyro measurements.

The satellite is equipped with the set of actuators summarized in Table 2. A 100 W class

Hall effect thruster [15, 16] is employed to compensate the secular variation in the orbit semi-major axis, caused by the in-track component of atmospheric drag. Simulation results indicate that the thrust needed to continuously counteract the drag force, for the considered mission scenario, is in the throttling range of such kind of thruster, and comparable to that required in similar missions, like GOCE (see, e.g., [7]). A 30 W Xenon resistojet [17] provides out of plane impulsive burns to compensate for the cross-track component of drag, which is due to the co-rotation of the atmosphere with the Earth, and the sun-synchronous resonance effects on the orbit inclination and right ascension of the ascending node. This kind of design is basically a trade-off between the thrust efficiency and the limitations imposed by the satellite payload and available power. In fact, we can take advantage of the Hall thruster high specific impulse to reduce the propellant consumption for drag compensation, which is the dominant factor in the mission delta-v budget, while using a higher thrust, low-power resistojet to counteract smaller cross-track perturbations, at the price of a very low specific impulse. Moreover, a single propellant tank containing Xenon gas will be shared between the Hall effect thruster and the resistojet, resulting in a simplified satellite internal layout. Finally, three momentum wheels produce the torques needed for attitude control. The spacecraft orientation is required to be aligned with the nominal attitude with a maximum absolute error of  $0.2^\circ$  per axis.

**Table 2 Actuators**

<i>Propulsion</i>	X axis	Y axis	Z axis
Type	100 W HET	30 W R.jet	-
Specific Impulse	$\sim 1000$ s	50 s	-
Thrust range	2.5 – 6 mN	10 – 50 mN	-
<i>Attitude</i>			
Type	1 Momentum Wheel per axis		

### C. Spacecraft and power system

In order to assess the feasibility of the proposed propulsion scheme, within the considered mission, a sketch of the spacecraft size, mass and power system is provided.



The external layout of the spacecraft is modeled as a rectangular box, with a square cross-section of  $0.5 \times 0.5 \text{ m}^2$  and a length of 1 m or more, similar to the elongated shape of the GOCE spacecraft. The assumed aerodynamic drag coefficient is 2.5.

The total mass of the spacecraft is assumed to be 100 kg, including 12 kg of propellant mass. The Hall thruster, the cathode and the Power Conditioning Unit (PCU) have a mass of less than 3 kg. The mass of the Xenon resistojet plus its power regulator can be estimated in 1 kg. The tank storing up to 12 liters of Xenon and all the valves, tubing, harness can be limited to additional 3 kg. Therefore, the propulsion system has a dry mass of less than 7 kg. Including the propellant, the whole propulsion system mass will not exceed 20 kg, i.e. about 20% of the total spacecraft mass.

Power is supplied by triple junction solar cells with an efficiency of about 28%, a packing factor of 0.85, and a 3% power degradation over the expected mission life. Given these figures, it is possible to consider solar arrays with a surface area of less than  $0.4 \text{ m}^2$  and a mass of about 2 kg, able to provide at least 100 W power at end of life. The external layout of the spacecraft can host a solar array installation of at least  $1 \text{ m}^2$ , whose total supplied power is largely sufficient for the proposed payload and propulsion needs. A battery system of 150 Wh/kg based on Li-ion cells is feasible for the proposed design.

The Hall thruster system is operated so that the supplied thrust can be changed about every 10 seconds. Several approaches have been proposed in literature in order to provide fast response times for this class of thrusters. Fast flow control valves (e.g. piezoelectric valves or digital MEMS actuators) can be used to quickly change the propellant flow, which in turn provides changes in the thrust (for fixed anode voltage). As an alternative, a high frequency variation (more than 10 Hz), can be obtained by pulse width modulation [18, 19]. Thrust variation can also be obtained by operating on the anode voltage through the PCU, at fixed propellant flow rate. This is the approach we refer to in this work and is feasible for the required 0.1 Hz variation rate. Indeed, for the thrust range reported in Table 2, given the Hall thruster technology characteristic, a minimum thrust of 2.5 mN can be obtained with about 40 W power (e.g., 200 V and 0.2 A). A 200 V applied voltage provides a specific impulse of more than 1000 s, as expected. For a 6 mN thrust, one can increase the applied voltage to about 500 V, keeping constant the propellant flow rate, and therefore the

current. Then, the specific impulse will significantly increase over the assumed 1000 s.

### III. Spacecraft model

This section describes the 6-DoF nonlinear simulation model that has been developed for the proposed mission scenario. This model includes the perturbed translational and rotational spacecraft dynamics, sensors and actuators.

#### A. Reference frames

Two Earth centered and two spacecraft centered coordinate frames are used in this work for the simulation of point mass and attitude dynamics, respectively. The Earth centered frames are the inertial (ECI) and the Earth fixed (ECEF) frames. The satellite centered frames are the Frenet and body-fixed frames. Vectors with capital letters as superscripts indicate the coordinate frame representation of the vector. Vectors with no superscripts are intended in the inertial reference frame. Rotations between two frames are expressed by rotation matrices  $\mathbf{R}$  or quaternions  $\mathbf{q}$ . The scalar portion of the quaternion is the first element and the quaternion multiplication is defined such that  $\mathbf{q}_{AC} = \mathbf{q}_{BC} \circ \mathbf{q}_{AB}$  corresponds to the sequence of rotations  $\mathbf{R}_{AC} = \mathbf{R}_{BC} \mathbf{R}_{AB}$ .

#### B. Spacecraft dynamics

The simulation model state is a 14-dimensional vector which includes the inertial position  $\mathbf{r}$  and velocity  $\mathbf{v}$ , the quaternion  $\mathbf{q}_{IB}$  defining the orientation of the spacecraft with respect to the inertial frame, the spacecraft angular rate  $\boldsymbol{\omega}^B$  defined in the spacecraft body reference frame, and the spacecraft mass  $m$ . The equations which describe the dynamics of the state vector are:

$$\dot{\mathbf{r}} = \mathbf{v} \quad (1)$$

$$\dot{\mathbf{v}} = -\mu \frac{\mathbf{r}}{\|\mathbf{r}\|^3} + \mathbf{a}_g + \mathbf{a}_d + \mathbf{a}_e + \frac{\mathbf{p}_u}{m} \quad (2a)$$

$$\mathbf{v}^\uparrow = \mathbf{v}^\downarrow + \Delta \mathbf{v}_u \quad (2b)$$

$$\dot{\mathbf{q}}_{IB} = \frac{1}{2} \begin{bmatrix} 0 \\ \boldsymbol{\omega}^B \end{bmatrix} \circ \mathbf{q}_{IB} \quad (3)$$

$$\dot{\boldsymbol{\omega}}^B = \mathbf{I}^{-1} (\boldsymbol{\tau}_g^B + \boldsymbol{\tau}_d^B + \boldsymbol{\tau}_e^B + \boldsymbol{\tau}_u^B - [\boldsymbol{\omega}^B \times] \mathbf{I} \boldsymbol{\omega}^B) \quad (4)$$

$$\dot{m} = - \frac{\|\mathbf{p}_u\|}{g I} \quad (5a)$$

$$m^\uparrow = \frac{m^\downarrow}{e^{\|\Delta \mathbf{v}_u\|/g I}} \quad (5b)$$

The considered orbit disturbance effects are due to the main perturbations acting on spacecrafts at low altitudes [20]. The gravitational and drag perturbations are specified by the disturbance accelerations  $\mathbf{a}_g$ ,  $\mathbf{a}_d$  and torques  $\boldsymbol{\tau}_g$ ,  $\boldsymbol{\tau}_d$ . The minor perturbations, such as solar radiation pressure (SRP), luni-solar attraction and magnetic disturbances, are accounted for through the terms  $\mathbf{a}_e$  and  $\boldsymbol{\tau}_e$ . The perturbations are computed according to the following mathematical models.

- Earth's non-spherical gravity field: A spherical harmonic expansion EGM96 [21] up to degree and order 24 for the disturbance acceleration and a spherical mass distribution for the gravity gradient torque computation are considered.
- Atmospheric drag: The Jacchia-71 model [22] is employed to approximate the atmospheric density. High solar activity ( $F_{10.7} = 220$ ) is considered, providing a worst-case scenario for the simulation. The drag force acting on the satellite is computed using the mean cross-sectional area, while the aerodynamic torque depends on the satellite layout and orientation [23].
- Solar radiation pressure: The solar radiation pressure value accounts for the Earth's orbit eccentricity and eclipse conditions [24]. A Cannonball model is employed for the translational dynamics while the solar radiation torque is related to the offset between the satellite center of pressure and center of mass.
- Earth's magnetic field: Magnetic disturbance torques result from the interaction of the spacecraft residual magnetic field and the geomagnetic field, described by the IGRF95 model truncated to degree and order 9 [25].
- Luni-solar attraction: Disturbance accelerations due to lunar and solar point mass gravity field are considered. The position of the Sun and the Moon is obtained through precise ephemerides [26].

### C. Sensors

Based on the sensing configuration described in Section II B, GPS position measurements are used for absolute position estimation. For attitude determination, combined continuous gyro measurements and discrete star-tracker measurements are employed [27].

#### 1. GPS

A GPS receiver supplies position measurements to the navigation filter. The measured spacecraft absolute position from the GPS is modeled as the true absolute position (in the ECEF frame) plus sensor noise  $\mathbf{w}_r^E$ :

$$\check{\mathbf{r}}^E = \mathbf{R}_{IE} \mathbf{r} + \mathbf{w}_r^E. \quad (6)$$

The covariance of the GPS noise, in absence of dilution of precision information, is assumed to be:

$$E[\mathbf{w}_r^E(t_k) \mathbf{w}_r^E(t_{k'})^T] = \mathbf{S}_r \delta_{kk'} = \sigma_r^2 \mathbf{I}_{3 \times 3} \delta_{kk'}. \quad (7)$$

#### 2. Gyro

The gyro model is based upon a package of three orthogonal strapdown gyros, each measuring the spacecraft angular velocity along its input axis. The input axes are chosen to be coincident with the spacecraft body axes. The measured angular rate  $\check{\boldsymbol{\omega}}^B$  is defined in terms of the true angular rate  $\boldsymbol{\omega}^B$  and measurement uncertainties. These include white Gaussian noise  $\mathbf{w}_\omega^B$ , gyro bias  $\mathbf{b}_\omega^B$ , scale factor bias  $f_\omega$  and gyro misalignment  $\boldsymbol{\epsilon}_\omega^B$ :

$$\check{\boldsymbol{\omega}}^B = (\mathbf{I}_{3 \times 3} - [\boldsymbol{\epsilon}_\omega^B \times]) [(1 + f_\omega) \boldsymbol{\omega}^B + \mathbf{b}_\omega^B + \mathbf{w}_\omega^B]. \quad (8)$$

The gyro bias is modeled as a Ornstein-Uhlenbeck process with a large time constant  $\tau_b$  [28]:

$$\dot{\mathbf{b}}_\omega^B = -\frac{\mathbf{b}_\omega^B}{\tau_b} + \mathbf{w}_{bd}^B. \quad (9)$$

The covariances of the white-noise processes  $\mathbf{w}_\omega^B$  and  $\mathbf{w}_{bd}^B$  are:

$$E[\mathbf{w}_\omega^B(t) \mathbf{w}_\omega^B(t')^T] = \mathbf{Q}_\omega \delta(t - t') = \sigma_\omega^2 \mathbf{I}_{3 \times 3} \delta(t - t'), \quad (10)$$

$$E[\mathbf{w}_{bd}^B(t) \mathbf{w}_{bd}^B(t')^T] = \mathbf{Q}_{bd} \delta(t - t') = \sigma_{bd}^2 \mathbf{I}_{3 \times 3} \delta(t - t'). \quad (11)$$

### 3. Star-tracker

The star-tracker measures the absolute orientation of the spacecraft. The star-tracker frame is supposed to be aligned with respect to the spacecraft body frame . Sensor noise is modeled as a small rotation vector  $\mathbf{w}_\theta^B$  [28]. The output of the star-tracker is thus a quaternion of the form:

$$\check{\mathbf{q}}_{IB} = \delta \mathbf{q}(\mathbf{w}_\theta^B) \circ \mathbf{q}_{IB} \quad (12)$$

where  $\delta \mathbf{q}(\mathbf{w}_\theta^B) \approx [1, \mathbf{w}_\theta^B/2]^T$  and the measurement noise covariance is:

$$E[\mathbf{w}_\theta^B(t_k) \mathbf{w}_\theta^B(t_{k'})^T] = \mathbf{S}_\theta \delta_{k k'} = \sigma_\theta^2 \mathbf{I}_{3 \times 3} \delta_{k k'} . \quad (13)$$

## D. Actuators

The satellite is equipped with the set of actuators reported in Table 2: momentum wheels for attitude control and a hybrid electric thruster (Hall effect and resistojet) for translational control. The propulsion system is supposed to be aligned with the satellite body axes, so that control torques and accelerations are uncoupled.

### 1. Hall effect thruster

A low power Hall effect thruster is employed for the along-track maneuvers. The thrust provided by the Hall effect thruster is obtained from the commanded thrust  $p_c$ , considering the following sources of error: actuator noise  $w_p$ , scale factor bias  $f_p$  and thrust alignment error  $\epsilon_p^B$ . The thrust vector, expressed in the inertial reference frame, is:

$$\mathbf{p}_u = \mathbf{R}(\mathbf{q}_{IB}^*) (\mathbf{I}_{3 \times 3} - [\epsilon_p^B \times]) \begin{bmatrix} (1 + f_p) p_c + w_p \\ 0 \\ 0 \end{bmatrix} . \quad (14)$$

The covariance of the thrust noise is:

$$E[w_p(t) w_p(t')] = \sigma_p^2 \delta(t - t') . \quad (15)$$

### 2. Resistojet

A low power resistojet, aligned with the cross-track direction, is employed to control the orbital plane inclination and the right ascension of the ascending node. The thrust is applied in short

bursts. Other sources of acceleration are considered negligible, so that one burst is approximated by an impulsive velocity change  $\Delta \mathbf{v}_u$ . The impulsive  $\Delta \mathbf{v}_u$  is obtained from the commanded  $\Delta v_c$ , including error sources such as thruster noise  $w_{\Delta v}$ , scale factor bias  $f_{\Delta v}$  and thrust alignment error  $\epsilon_{\Delta v}^B$ :

$$\Delta \mathbf{v}_u = \mathbf{R}(\mathbf{q}_{IB}^*) (\mathbf{I}_{3 \times 3} - [\epsilon_{\Delta v}^B \times]) \begin{bmatrix} 0 \\ (1 + f_{\Delta v}) \Delta v_c + w_{\Delta v} \\ 0 \end{bmatrix}. \quad (16)$$

The covariance of the impulsive thruster noise is:

$$E[w_{\Delta v}(t_k) w_{\Delta v}(t_{k'})] = \sigma_{\Delta v}^2 \delta_{kk'}. \quad (17)$$

### 3. Momentum wheels

Momentum wheels provide the torques  $\tau_u^B$  needed to change the attitude of the satellite. The considered attitude control strategy requires the generated torques to be independent, with respect to the satellite body axes. Hence there is one momentum wheel per axis. The torque generated by the momentum wheels, for a commanded torque  $\tau_c^B$ , includes actuator noise  $\mathbf{w}_\tau^B$ , scale factor bias  $f_\tau$  and misalignment error  $\epsilon_\tau^B$ :

$$\tau_u^B = (\mathbf{I}_{3 \times 3} - [\epsilon_\tau^B \times]) [(1 + f_\tau) \tau_c^B + \mathbf{w}_\tau^B]. \quad (18)$$

The covariance of the momentum wheels noise is:

$$E[\mathbf{w}_\tau^B(t) \mathbf{w}_\tau^B(t')^T] = \sigma_\tau^2 \mathbf{I}_{3 \times 3} \delta(t - t'). \quad (19)$$

## IV. Guidance, navigation and control

The proposed GNC system includes autonomous orbit and attitude determination and control algorithms. The navigation solution is an extended Kalman filter based on a simplified spacecraft dynamic model, which provides estimates of the spacecraft absolute position and attitude. The autonomous orbit control problem is formulated as a leader-follower formation flying control problem in which one spacecraft is virtual and not affected by non-gravitational perturbations as in [14]. To this aim, a reference trajectory is numerically computed from the nominal orbital elements. An

efficient thrusting strategy is then developed using mean orbital elements control theory, while attitude control is carried out using a proportional derivative feedback law. Figure 1 shows the block diagram representation of the GNC system.

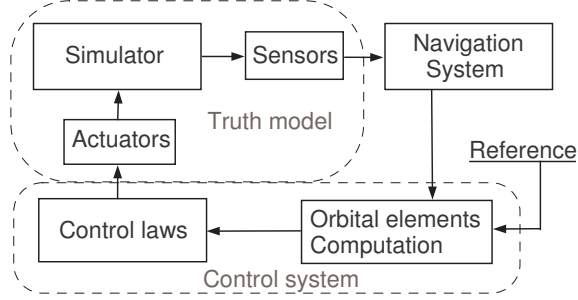


**Fig. 1 Block diagram representation of the GNC system.**

### A. Navigation

A continuous-discrete extended Kalman filter is adopted for autonomous navigation [29]. The navigation filter processes GPS measurements and attitude data from gyros and a star tracker to estimate absolute position, velocity and attitude of the spacecraft. The navigation state is a 13-dimensional vector, which includes the inertial position  $\hat{\mathbf{r}}$ , the inertial velocity  $\hat{\mathbf{v}}$ , the quaternion  $\hat{\mathbf{q}}_{IB}$  defining the orientation of the spacecraft with respect to the inertial frame, and the gyro bias  $\hat{\mathbf{b}}_{\omega}^B$ . The filter state does not contain angular velocity and mass. The difference between the gyro output and the estimated gyro bias is used as an estimate of the angular velocity state [28]:

$$\hat{\boldsymbol{\omega}}^B = \tilde{\boldsymbol{\omega}}^B - \hat{\mathbf{b}}_{\omega}^B. \quad (20)$$

Mass is assumed to be directly measured by on-board instruments. The dynamic model used to propagate the navigation state is:

$$\dot{\hat{\mathbf{r}}} = \hat{\mathbf{v}} \quad (21)$$

$$\dot{\hat{\mathbf{v}}} = -\mu \frac{\hat{\mathbf{r}}}{\|\hat{\mathbf{r}}\|^3} + \mathbf{a}_{J2}(\hat{\mathbf{r}}) \quad (22)$$

$$\dot{\hat{\mathbf{q}}}_{IB} = \frac{1}{2} \begin{bmatrix} 0 \\ \hat{\boldsymbol{\omega}}^B \end{bmatrix} \circ \hat{\mathbf{q}}_{IB} \quad (23)$$

$$\dot{\hat{\mathbf{b}}}_{\omega}^B = -\frac{\hat{\mathbf{b}}_{\omega}^B}{\tau_b} \quad (24)$$

where the estimate  $\mathbf{a}_{J2}(\hat{\mathbf{r}})$  of the gravitational disturbance acceleration  $\mathbf{a}_g$ , in equation (2a), accounts only for the J2 harmonic of the gravity field, which is the major perturbing term. It should be noticed that no control and drag accelerations are considered in equation (22), because the resultant from the interaction of the thrust acceleration  $\mathbf{p}_u/m$  with the aerodynamic drag  $\mathbf{a}_d$  is assumed to be negligible for the considered mission scenario. The disturbance term  $\mathbf{a}_e$  in equation (2a), which represents the effects of the minor orbital perturbations, is also neglected. The uncertainty introduced by these assumption is modeled as white process noise  $\mathbf{w}_a$ , with covariance given by:

$$E[\mathbf{w}_a(t) \mathbf{w}_a(t')^T] = \mathbf{Q}_a = \sigma_a^2 \mathbf{I}_{3 \times 3} \delta(t - t'). \quad (25)$$

To avoid covariance singularities due to the quaternion unit-norm constraint, a modified estimation error vector  $\mathbf{m}$  is adopted to propagate the covariance matrix and to update both the state and the covariance matrix of the filter:

$$\mathbf{m} = \begin{bmatrix} \delta \mathbf{r} \\ \delta \mathbf{v} \\ \boldsymbol{\theta}^B \\ \delta \mathbf{b}_\omega^B \end{bmatrix} \quad (26)$$

In the modified estimation error vector, the attitude error is parametrized by the three-dimensional rotation vector  $\boldsymbol{\theta}^B$ , instead of being expressed in quaternion form [28]. If the quaternion estimation error is small, it can be approximated as:

$$\delta \mathbf{q}(\boldsymbol{\theta}^B) = \mathbf{q}_{IB} \circ \hat{\mathbf{q}}_{IB}^* \approx \begin{bmatrix} 1 \\ \boldsymbol{\theta}^B/2 \end{bmatrix} \quad (27)$$

Using the linearized Bortz equation [30] and assuming that gyro scale factor bias and misalignment errors in equation (8) are negligible with respect to gyro noise, it is possible to approximate the attitude error dynamics as:

$$\begin{aligned} \dot{\boldsymbol{\theta}}^B &= \delta \boldsymbol{\omega}^B - \hat{\boldsymbol{\omega}}^B \times \boldsymbol{\theta}^B \\ \delta \boldsymbol{\omega}^B &= \boldsymbol{\omega}^B - \hat{\boldsymbol{\omega}}^B \approx -(\mathbf{w}_\omega^B + \delta \mathbf{b}_\omega^B). \end{aligned} \quad (28)$$

The covariance matrix  $\mathbf{P} = E[\mathbf{m} \mathbf{m}^T]$  of the filter is propagated according to:

$$\dot{\mathbf{P}} = \mathbf{F} \mathbf{P} + \mathbf{P} \mathbf{F}^T + \mathbf{Q}. \quad (29)$$



Making use of equation (28) together with the model equations (21), (22) and (24), the modified Jacobian matrix  $\mathbf{F}$  can be expressed, with respect to  $\mathbf{m}$ , as:

$$\mathbf{F} = \begin{bmatrix} \mathbf{0}_{3 \times 3} & \mathbf{I}_{3 \times 3} & \mathbf{0}_{3 \times 3} & \mathbf{0}_{3 \times 3} \\ \partial \hat{\mathbf{v}} / \partial \hat{\mathbf{r}} & \mathbf{0}_{3 \times 3} & \mathbf{0}_{3 \times 3} & \mathbf{0}_{3 \times 3} \\ \mathbf{0}_{3 \times 3} & \mathbf{0}_{3 \times 3} & -[\hat{\boldsymbol{\omega}}^B \times] & -\mathbf{I}_{3 \times 3} \\ \mathbf{0}_{3 \times 3} & \mathbf{0}_{3 \times 3} & \mathbf{0}_{3 \times 3} & -\frac{1}{\tau_b} \mathbf{I}_{3 \times 3} \end{bmatrix}. \quad (30)$$

The process noise covariance is a block diagonal matrix  $\mathbf{Q}$  defined by:

$$\mathbf{Q} = \text{blockdiag}(\mathbf{0}_{3 \times 3}, \mathbf{Q}_a, \mathbf{Q}_\omega, \mathbf{Q}_{bd}) \quad (31)$$

where  $\mathbf{Q}_a$ ,  $\mathbf{Q}_\omega$  and  $\mathbf{Q}_{bd}$  are given by equations (25), (10) and (11), respectively. When an impulsive  $\Delta \mathbf{v}$  maneuver occurs, the filter state vector and covariance matrix must be modified according to equations (2b)-(16):

$$\hat{\mathbf{v}}^\uparrow = \hat{\mathbf{v}}^\downarrow + \Delta \hat{\mathbf{v}}_u \quad (32)$$

$$\mathbf{P}^\uparrow = \mathbf{D} \mathbf{P}^\downarrow \mathbf{D}^T + \mathbf{Q}_D \quad (33)$$

where the estimated velocity change vector  $\Delta \hat{\mathbf{v}}_u = \mathbf{R}(\hat{\mathbf{q}}_{IB}^*) [0, \Delta v_c, 0]^T$  is obtained from equation (16), neglecting the resistojet scale factor and alignment errors. The correction term  $\mathbf{D}$  and  $\mathbf{Q}_D$  are given by:

$$\mathbf{D} = \begin{bmatrix} \mathbf{I}_{3 \times 3} & \mathbf{0}_{3 \times 3} & \mathbf{0}_{3 \times 3} & \mathbf{0}_{3 \times 3} \\ \mathbf{0}_{3 \times 3} & \mathbf{I}_{3 \times 3} & \mathbf{R}(\hat{\mathbf{q}}_{IB}^*) [\Delta \hat{\mathbf{v}}_u^B \times] & \mathbf{0}_{3 \times 3} \\ \mathbf{0}_{3 \times 3} & \mathbf{0}_{3 \times 3} & \mathbf{I}_{3 \times 3} & \mathbf{0}_{3 \times 3} \\ \mathbf{0}_{3 \times 3} & \mathbf{0}_{3 \times 3} & \mathbf{0}_{3 \times 3} & \mathbf{I}_{3 \times 3} \end{bmatrix} \quad (34)$$

$$\mathbf{Q}_D = \text{blockdiag}(\mathbf{0}_{3 \times 3}, \mathbf{Q}_{\Delta v}, \mathbf{0}_{3 \times 3}, \mathbf{0}_{3 \times 3}) \quad (35)$$

where

$$\mathbf{Q}_{\Delta v} = \mathbf{R}(\hat{\mathbf{q}}_{IB}^*) \text{diag}(0, \sigma_{\Delta v}^2, 0) \mathbf{R}(\hat{\mathbf{q}}_{IB}). \quad (36)$$

When measurements are available, the attitude estimate is updated by using a multiplicative approach, while the classical update equations are adopted for the other states:

$$\begin{bmatrix} \hat{\mathbf{r}}^+ \\ \hat{\mathbf{v}}^+ \\ \hat{\mathbf{q}}_{IB}^+ \\ \hat{\mathbf{b}}_\omega^{B+} \end{bmatrix} = \begin{bmatrix} \delta\hat{\mathbf{r}}^+ + \hat{\mathbf{r}}^- \\ \delta\hat{\mathbf{v}}^+ + \hat{\mathbf{v}}^- \\ \delta\mathbf{q}(\hat{\boldsymbol{\theta}}^{B+}) \circ \hat{\mathbf{q}}_{IB}^- \\ \delta\hat{\mathbf{b}}_\omega^{B+} + \hat{\mathbf{b}}_\omega^{B-} \end{bmatrix} \quad (37)$$

where

$$\begin{bmatrix} \delta\hat{\mathbf{r}}^+ \\ \delta\hat{\mathbf{v}}^+ \\ \hat{\boldsymbol{\theta}}^{B+} \\ \delta\hat{\mathbf{b}}_\omega^{B+} \end{bmatrix} = \mathbf{K}\tilde{\mathbf{z}}. \quad (38)$$

The filter covariance is updated according to:

$$\mathbf{P}^+ = (\mathbf{I}_{12 \times 12} - \mathbf{K}\mathbf{H})\mathbf{P}^- \quad (39)$$

$$\mathbf{K} = \mathbf{P}^-\mathbf{H}^T(\mathbf{H}\mathbf{P}^-\mathbf{H}^T + \mathbf{S})^{-1}. \quad (40)$$

The measurement noise covariance matrix  $\mathbf{S}$  is generated according to the noise covariances associated to the measurements used in the update step (GPS, star-tracker), as specified in Section III C.

The measurement residuals  $\tilde{\mathbf{z}}$  and the observation models  $\mathbf{H}$  used by the filter are given next.

#### 1. GPS measurements

The measurement residual for the GPS measurements is expressed as:

$$\tilde{\mathbf{z}}_r = \check{\mathbf{r}}^E - \hat{\mathbf{r}}^E. \quad (41)$$

The Kalman filter estimate of the GPS measurements is based on the model of equation (6):

$$\hat{\mathbf{r}}^E = \mathbf{R}_{IE} \hat{\mathbf{r}}^- \quad (42)$$

where the rotation from the inertial to the ECEF frame is supposed to be known. Hence, the GPS measurement matrix is simply given by:

$$\mathbf{H}_r = [\mathbf{R}_{IE} \quad \mathbf{0}_{3 \times 9}]. \quad (43)$$

## 2. Star-tracker measurements

A simple way to present the information in the measured quaternion to the Kalman filter is in terms of the three dimensional rotation vector parametrizing the estimated attitude error. Therefore a *derived* measurement [28] is calculated, which expresses the measurement residual as follows:

$$\begin{bmatrix} 1 \\ \tilde{\mathbf{z}}_\theta/2 \end{bmatrix} \approx \delta \mathbf{q}(\tilde{\mathbf{z}}_\theta) = \check{\mathbf{q}}_{IB} \circ \hat{\mathbf{q}}_{IB}^{*-}. \quad (44)$$

The estimated star tracker measurements can be defined, with respect to the error state vector, as:

$$\hat{\mathbf{z}}_\theta = \hat{\boldsymbol{\theta}}^{B-} = \mathbf{H}_\theta \hat{\mathbf{m}}^- \quad (45)$$

where  $\mathbf{H}_\theta = [\mathbf{0}_{3 \times 6} \quad \mathbf{I}_{3 \times 3} \quad \mathbf{0}_{3 \times 3}]$ . It should be noticed that  $\tilde{\mathbf{z}}_\theta = \check{\boldsymbol{\theta}}^B$ , since  $\hat{\boldsymbol{\theta}}^{B-} = 0$  in the pre-update phase.

## B. Guidance

Based on the nominal orbit and attitude, described in Section II A, the guidance algorithm specifies the desired spacecraft inertial position and velocity, as well as its orientation and angular velocity.

### 1. Reference trajectory

The osculating reference trajectory is computed by integrating the following spacecraft equations of motion:

$$\dot{\bar{\mathbf{r}}} = \bar{\mathbf{v}} \quad (46)$$

$$\dot{\bar{\mathbf{v}}} = -\mu \frac{\bar{\mathbf{r}}}{\|\bar{\mathbf{r}}\|^3} + \mathbf{a}_g(\bar{\mathbf{r}}). \quad (47)$$

The gravitational disturbances are included in the reference dynamics through the acceleration term  $\mathbf{a}_g(\bar{\mathbf{r}})$ , which accounts for the Earth's non-spherical gravity field, modeled using the spherical harmonic expansion EGM96 up to degree and order 9. The initial integration condition is obtained from the initial orbital elements, shown in Table 1. These mean orbital elements are first converted to the corresponding osculating orbit elements, according to Brouwer's artificial satellite theory [31], then the well-known transformation between osculating orbital elements and inertial states (position, velocity) is applied [32].

## 2. Reference attitude

The reference attitude depends only on the current inertial position and velocity of the spacecraft, thus it is independent from the reference trajectory. Based on the filter estimates, the rotation matrix from the inertial to the Frenet reference frame can be expressed as:

$$\hat{\mathbf{R}}_{IF} = \left[ \frac{\hat{\mathbf{v}}}{\|\hat{\mathbf{v}}\|}, \frac{\hat{\mathbf{r}} \times \hat{\mathbf{v}}}{\|\hat{\mathbf{r}} \times \hat{\mathbf{v}}\|}, \frac{\hat{\mathbf{v}}}{\|\hat{\mathbf{v}}\|} \times \frac{\hat{\mathbf{r}} \times \hat{\mathbf{v}}}{\|\hat{\mathbf{r}} \times \hat{\mathbf{v}}\|} \right]^T. \quad (48)$$

For attitude control purposes, the reference attitude is parametrized by a quaternion:

$$\bar{\mathbf{q}}_{IB} = \mathbf{q}(\hat{\mathbf{R}}_{IF}). \quad (49)$$

The angular rate of the spacecraft has finally to match the Frenet frame rotation rate  $\boldsymbol{\omega}_F^F$ , expressed in the body frame:

$$\bar{\boldsymbol{\omega}}^B = \mathbf{R}(\hat{\mathbf{q}}_{IB}) \hat{\mathbf{R}}_{IF}^T \boldsymbol{\omega}_F^F. \quad (50)$$

For a nearly circular orbit, the Frenet frame rotation rate around its Y axis can be approximated as:

$$\boldsymbol{\omega}_F^F \approx [0, \|\hat{\mathbf{v}}\|/\|\hat{\mathbf{r}}\|, 0]^T. \quad (51)$$

## C. Control

### 1. Orbital station-keeping

The autonomous orbit control problem has been addressed in the literature using feedback control laws based on either Cartesian coordinates [33] or orbital elements [14]. Cartesian feedback laws are typically suitable for drag compensation of very low Earth orbit satellites, demanding a continuous thrust, whereas orbital elements feedback laws can be applied to general-purpose station-keeping maneuvers, using continuous and impulsive thrusters. The propulsion system considered in this paper consists of electric propulsion devices nominally aligned to the Frenet frame, with no thrust available in the normal direction. This configuration limits the use of Cartesian control laws, which cannot be easily modified to account for a lack of normal thrust. Therefore an orbital elements based control is adopted. Following the same approach taken in [34], the control law is formulated in terms of mean orbital elements, rather than osculating orbital elements, so that

differential oscillation (with respect to the virtual spacecraft on the reference orbit) due to short periodic gravitational perturbations are not treated as tracking errors.

Based on the simplified Gauss' variational equations of motion, adapted for near-circular orbits [35], the mean orbital elements dynamics can be expressed as:

$$\dot{\mathbf{e}} \approx \mathbf{A}(\mathbf{e}) + \mathbf{B}(\mathbf{e}) \mathbf{a}_c^F \quad (52)$$

where  $\mathbf{e} = [a, e_x, e_y, i, \Omega, u]^T$  is the mean state vector and  $\mathbf{a}_c^F$  is the commanded acceleration in the Frenet frame, which is approximately aligned to an LVLH frame for the considered satellite orbit. The plant matrix  $\mathbf{A}(\mathbf{e})$  describes the uncontrolled behavior of the mean orbital elements and the control input matrix  $\mathbf{B}(\mathbf{e})$  is given by:

$$\mathbf{B}(\mathbf{e}) = \frac{1}{na} \begin{bmatrix} 2a & 0 & 0 \\ 2 \cos u & 0 & \sin u \\ 2 \sin u & 0 & -\cos u \\ 0 & \cos u & 0 \\ 0 & \sin u / \sin i & 0 \\ 0 & -\sin u \cot i & -2 \end{bmatrix} \quad (53)$$

where  $n = \sqrt{\mu/a^3}$  is the mean motion. The tracking error vector  $\delta \bar{\mathbf{e}}$  is defined as the difference between the reference and estimated mean orbital elements:

$$\delta \bar{\mathbf{e}} = \bar{\mathbf{e}} - \hat{\mathbf{e}}. \quad (54)$$

In order to compute  $\delta \bar{\mathbf{e}}$  in (54), the reference and estimated inertial states are first transformed into corresponding osculating elements  $\bar{\mathbf{e}}_o$  and  $\hat{\mathbf{e}}_o$ . Then, the osculating elements are converted to the corresponding mean elements  $\bar{\mathbf{e}}$  and  $\hat{\mathbf{e}}$  by using Brouwer's analytical transformation [31].

The problem of driving to zero the tracking errors  $\delta \bar{\mathbf{e}}$  can be tackled by using a nonlinear regulator in the form:

$$\mathbf{a}_c^F = \mathbf{B}(\hat{\mathbf{e}})^T \mathbf{K}_c \delta \bar{\mathbf{e}} \quad (55)$$

where  $\mathbf{K}_c$  is a diagonal matrix of positive gains [36]. If the gain matrix is large enough to compensate for differential disturbances  $(\mathbf{A}(\bar{\mathbf{e}}) - \mathbf{A}(\hat{\mathbf{e}}))$ , and perfect information ( $\hat{\mathbf{e}} = \mathbf{e}$ ) is assumed, this control

law guarantees asymptotic tracking of the reference orbital elements (see [34, 37] for a thorough Lyapunov-based theoretical analysis). Unfortunately, it demands continuous thrust along the in-track, cross track, and normal directions, while the propulsive scheme considered in this paper can provide limited continuous thrust only in the in-track direction. Therefore, an alternative hybrid continuous/impulsive control scheme is proposed in the following, by taking into account the structure of the matrix  $\mathbf{B}(\mathbf{e})$  and the specific features of the considered mission.

The proposed in-track control law is formulated by excluding cross-track and normal thrusting from the nonlinear controller of equation (55), which therefore takes on the form  $\mathbf{a}_c^F = [p_c/\tilde{m}, 0, 0]^T$ , where  $p_c$  is the commanded thrust in (14) and can be explicitly written as

$$p_c = \frac{\tilde{m}}{\hat{n} \hat{a}} \begin{bmatrix} 2\hat{a} \\ 2 \cos \hat{u} \\ 2 \sin \hat{u} \end{bmatrix}^T \begin{bmatrix} K_a \delta \bar{a} \\ K_{ex} \delta \bar{e}_x \\ K_{ey} \delta \bar{e}_y \end{bmatrix}$$

with  $\hat{n} = \sqrt{\mu/\hat{a}^3}$ . Such a control law has to be modified in order to compensate for the steady state tracking error of the semi-major axis arising from drag, which is a non-zero mean disturbance. This can be done by adding an integral term on the semi-major axis error. Then, according to (55) one has

$$p_c = \frac{\tilde{m}}{\hat{n} \hat{a}} \begin{bmatrix} 2\hat{a} \\ 2 \cos \hat{u} \\ 2 \sin \hat{u} \end{bmatrix}^T \begin{bmatrix} K_a \delta \bar{a} \\ K_{ex} \delta \bar{e}_x \\ K_{ey} \delta \bar{e}_y \end{bmatrix} + \tilde{m} K_I \int \delta \bar{a} dt, \quad (56)$$

where  $K_I$  is a positive gain. From equations (52)-(53), it follows that a lack of normal thrust, together with a nearly polar orbital inclination, results in an uncontrolled dynamics for the mean argument of latitude  $u$ . A possible way to overcome this issue is to force a different reference  $a'$  for the semi-major axis. Since for nearly circular orbits  $\dot{u} \approx \sqrt{\mu/a^3}$ , it can be verified that by choosing

$$a' = \left( K_u \delta \bar{u} + \sqrt{\frac{1}{\bar{a}^3}} \right)^{-2/3} \quad (57)$$

with  $K_u$  being a positive constant, results in an asymptotic stable dynamics for the mean argument of latitude error  $\delta \bar{u}$  [38]. Hence equation (56) must be modified by replacing  $\delta \bar{a}$  with  $\delta a' = a' - \hat{a}$ .

Notice that, from (57), when  $\delta\bar{u}$  vanishes the modified reference  $a'$  of the semi-major axis matches the reference value  $\bar{a}$ , and hence  $\delta a' = \delta\bar{a}$  as desired.

The inclination  $i$  and the right ascension of the ascending node  $\Omega$  are controlled via the cross-track impulsive control scheme (16) provided by the resistojet. From equations (52)-(53), it is evident that the efficiency of an impulsive cross-track maneuver for  $i$  and  $\Omega$  adjustments is maximized when the spacecraft passes through the equatorial ( $u = k\pi$ ) and polar ( $u = k\pi + \pi/2$ ) regions, respectively [39]. The proposed approach consists in applying a sequence of impulsive burns at  $\hat{u} = \pi$  or  $\hat{u} = \frac{3}{2}\pi$  whenever the tracking errors  $\delta\bar{i}$  or  $\delta\bar{\Omega}$  exceed a predefined control window. The sequence of burns is stopped when the corresponding tracking error reaches the lower bound of the control window. The commanded delta-v, corresponding to a single burn, is:

$$\Delta v_c = -(p_\Delta/\tilde{m}) \Delta t_v \quad (58)$$

where  $\Delta v_c$  is the commanded delta-v in (16),  $p_\Delta$  is the maximum nominal thrust of the resistojet and  $\Delta t_v$  is a small firing time.

## 2. Attitude control

Attitude control is carried out by using a classical proportional derivative feedback law. The commanded torques, needed to keep the nominal attitude, are given by:

$$\boldsymbol{\tau}_c^B = \mathbf{K}_\theta \bar{\boldsymbol{\theta}}^B + \mathbf{K}_\omega (\bar{\boldsymbol{\omega}}^B - \hat{\boldsymbol{\omega}}^B) \quad (59)$$

where the attitude tracking error is parametrized by the three-dimensional rotation vector  $\bar{\boldsymbol{\theta}}^B$ , which is obtained from the vector part of the attitude error quaternion as:

$$\begin{bmatrix} 1 \\ \bar{\boldsymbol{\theta}}^B/2 \end{bmatrix} \approx \delta \mathbf{q}(\bar{\boldsymbol{\theta}}^B) = \bar{\mathbf{q}}_{IB} \circ \hat{\mathbf{q}}_{IB}^* \quad (60)$$

## V. Simulation results

The reference mission has been simulated in order to validate the proposed GNC solution and to evaluate the performance of the hybrid propulsion system. The truth model, navigation state and reference dynamics are propagated for 20 days using a fourth-order Runge-Kutta integration method. The most significant navigation and control parameters are shown in Table 3, while the

specifications of sensors and actuators are summarized in Table 4. The standard deviation  $\sigma_{bd}$  in (11) has been computed from the standard deviation of the gyro bias  $\sigma_b$  available from the sensor specifications, according to the asymptotic relationship  $\sigma_{bd}^2 = 2\sigma_b^2/\tau_b$ , with  $\sigma_b = 1^\circ/\text{hr}$  and  $\tau_b = 2$  hr. The orbit control gains are selected in order to satisfy the Hall thruster output limitations and

**Table 3 Navigation and control parameters**

Process noise	
Unmodeled disturbances	$\sigma_a = 1 \text{ mm/s}^{3/2}$
Orbit control	
$\delta\bar{a}$ gain	$K_{a'} = 4 \cdot 10^{-11}$
$\delta\bar{e}_x, \delta\bar{e}_y$ gain	$K_{ex}, K_{ey} = 3 \cdot 10^3$
$\delta\bar{u}$ gain	$K_u = 10^{-12}$
Integral gain	$K_I = 3.5 \cdot 10^{-11}$
$\delta\bar{i}$ control window	$\pm 3.5 \cdot 10^{-5} \text{ rad}$
$\delta\bar{\Omega}$ control window	$[0, 3.5 \cdot 10^{-5}] \text{ rad}$
Impulsive firing time	$\Delta t_v = 20 \text{ s}$
Update time	10 s
Attitude control	
Proportional gain	$\mathbf{K}_\theta = 0.004 \mathbf{I}_{3 \times 3}$
Derivative gain	$\mathbf{K}_\omega = 0.18 \mathbf{I}_{3 \times 3}$
Update time	10 s

minimize the steady state oscillations due to estimation errors. The attitude control gains are found by comparing the linearized attitude dynamics with the second order equation of a mass-spring-damper system and expressing  $\mathbf{K}_\theta$  and  $\mathbf{K}_\omega$  as a function of the natural frequency and damping ratio of the system [23]. The update frequencies of sensors and control algorithms are set to rather conservative values to reduce the power requirement and computational burden of the GNC system.

#### A. Navigation system analysis

The performance of the proposed Kalman filtering scheme is evaluated in terms of the inertial position and attitude determination errors, shown together with their  $3\sigma$  confidence intervals in



**Table 4 Sensors and actuators specifications**

Device	Noise	Scale factor	Alignment error	Update frequency
Gyro	$\sigma_\omega = 0.02 \text{ mrad}/\sqrt{\text{s}}$ $\sigma_{bd} = 8.1 \cdot 10^{-8} \text{ rad}/\text{s}^{3/2}$	$f_\omega = 100 \text{ ppm}$	$\epsilon_\omega^B = 0.3 \text{ mrad}/\text{axis}$	Continuous
Star-tracker	$\sigma_\theta = 0.3 \text{ mrad}$	-	-	0.05 Hz
Gps	$\sigma_r = 30 \text{ m}$	-	-	0.1 Hz
Momentum wheels	$\sigma_\tau = 3 \cdot 10^{-5} \text{ N}\cdot\text{m}\sqrt{\text{s}}$	$f_\tau = 300 \text{ ppm}$	$\epsilon_\tau^B = 0.3 \text{ mrad}/\text{axis}$	Continuous
Hall thruster	$\sigma_p = 0.3 \text{ mN}\sqrt{\text{s}}$	$f_p = 300 \text{ ppm}$	$\epsilon_\tau^B = 0.3 \text{ mrad}/\text{axis}$	Continuous
Resistojet	$\sigma_{\Delta v} = 1 \text{ mm}/\text{s}$	$f_{\Delta v} = 300 \text{ ppm}$	$\epsilon_{\Delta v}^B = 0.3 \text{ mrad}/\text{axis}$	Impulsive

Figures 2-3. The filter state is initialized with the first attitude and position measurements. After

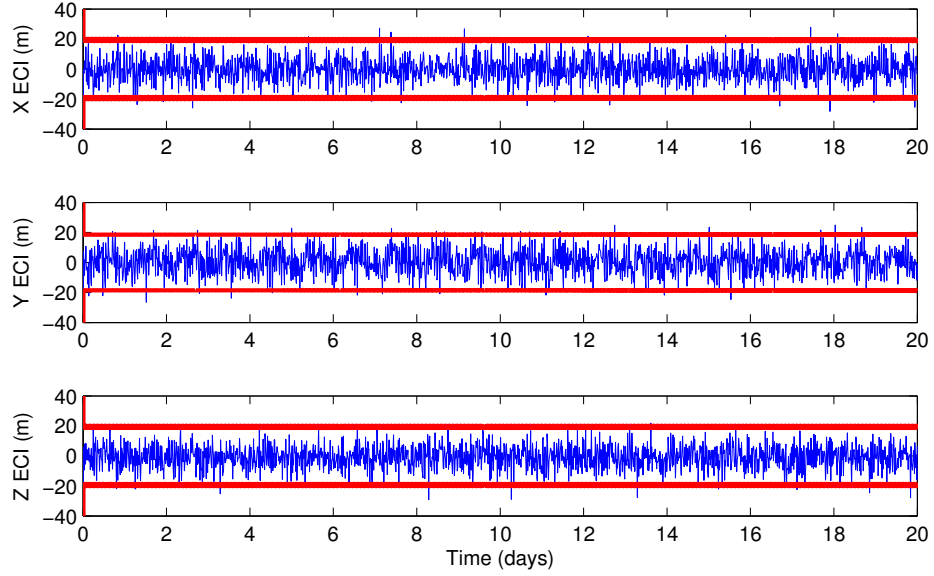


**Fig. 2 Inertial position estimation error and  $3\sigma$  confidence intervals.**

a short transient phase, each component of the  $3\sigma$  ECI position vector error drops to a steady state value of approximately 20 m. At the same time the  $3\sigma$  attitude error reaches a steady state value of about  $0.03^\circ$  per axis. In both cases the errors have approximately zero mean and remain within the confidence intervals most of the time.

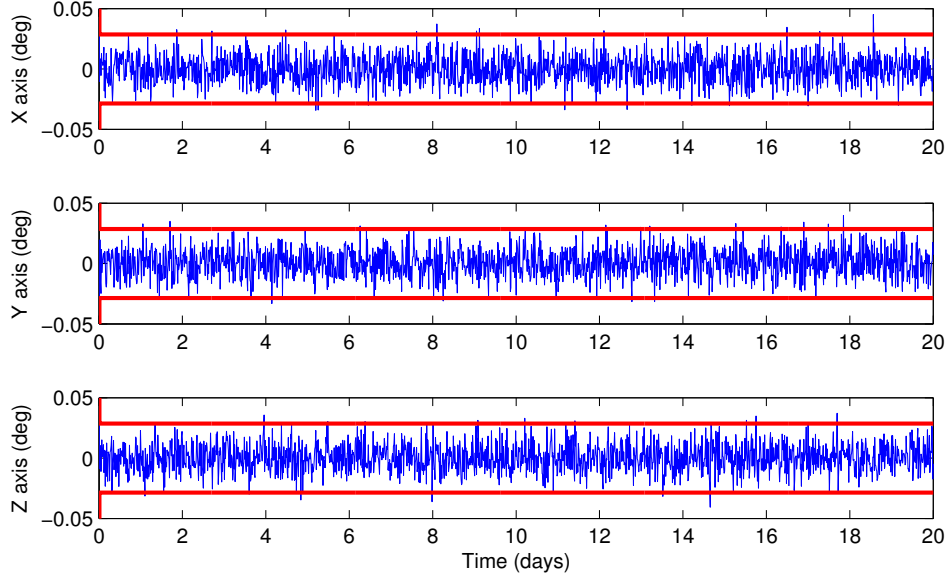


**Fig. 3 Attitude estimation error and  $3\sigma$  confidence intervals.**

#### B. Closed loop system analysis

The closed loop system analysis accounts for the effects of a realistic truth model, sensors, actuators and GNC flight algorithms. Since the orbit control requirements are specified in terms of inertial states, the control system performance is presented, in Figure 4, in terms of osculating position tracking error, even if the control laws are developed in the mean orbital element space. This is consistent with the reference trajectory generation scheme. The in-track component of the error, which is proportional to the mean argument of latitude error, has the major impact on the satellite distance from the reference orbit, being controlled passively with an accuracy of about 400 m. The cross-track component is strongly influenced by inclination and right ascension of the ascending node errors: the achieved 250 m accuracy is a function of the impulsive control window size. The normal component is controlled with the accuracy of less than 50 m, reflecting the semi-major axis error. Figure 5 shows the satellite distance from the reference orbit, whose root mean square value is 220 m (neglecting the transient phase). The attitude tracking error, whose components are bounded between  $\pm 0.2^\circ$ , is depicted in Figure 6. These results show that the control requirements are satisfied.

The performance of the proposed propulsion system is depicted in Figure 7, in terms of the

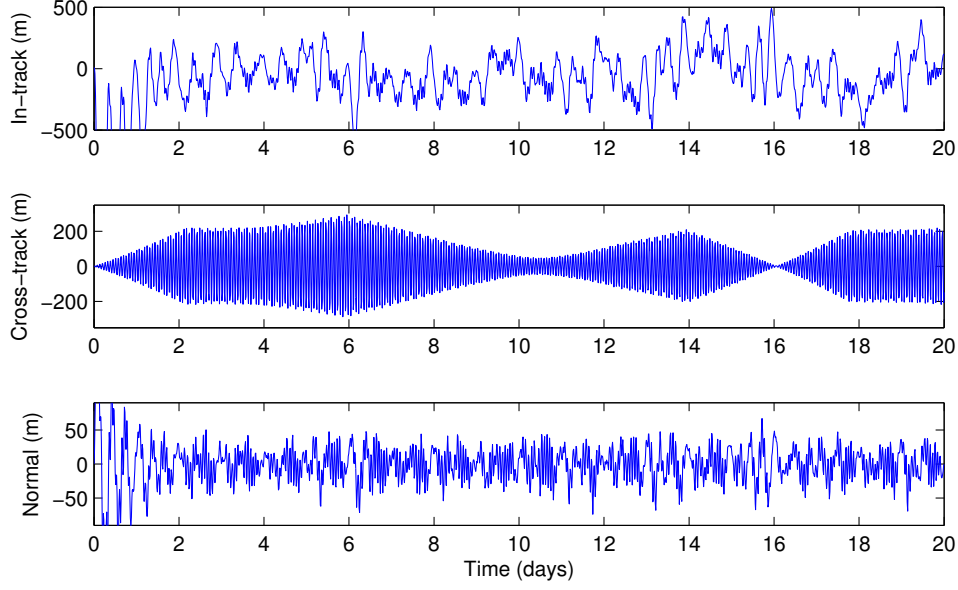


**Fig. 4 Position tracking error.**

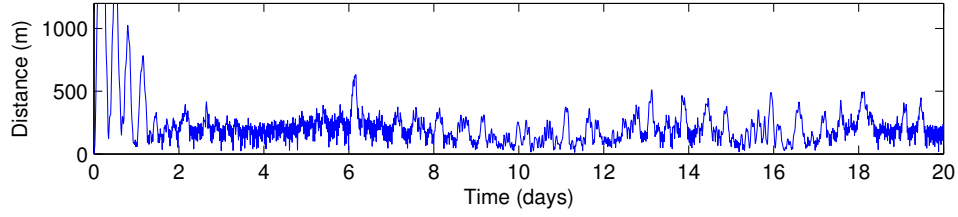


**Fig. 5 Distance from the reference orbit.**

Hall thruster and resistojet outputs and the Xenon propellant mass consumption. A continuous thrust with mean value of approximately 4 mN and delta-v impulses of about 10 mm/s magnitude, which corresponds to a 20 s burn at 50 mN, are required for orbital station-keeping. In the second plot of Figure 7, each burn is represented by a bullet. An increased density of bullets in the plot indicates that the resistojet is firing twice per orbit (at  $\hat{u} = \pi$  and  $3/2\pi$ ) rather than once (at  $\hat{u} = \pi$  or  $3/2\pi$ ), while the thruster is not firing in correspondence of empty spaces. Note that the power requirements for simultaneous use of the resistojet and the Hall thruster is about 140 W, which is fully compatible with the power system described in Section II C. The total propellant consumption is 1.19 kg, including 0.64 kg for continuous thrust and 0.55 kg for impulsive maneuvers. Considering a 12 kg propellant tank, the expected lifetime of the satellite is approximately 200 days.

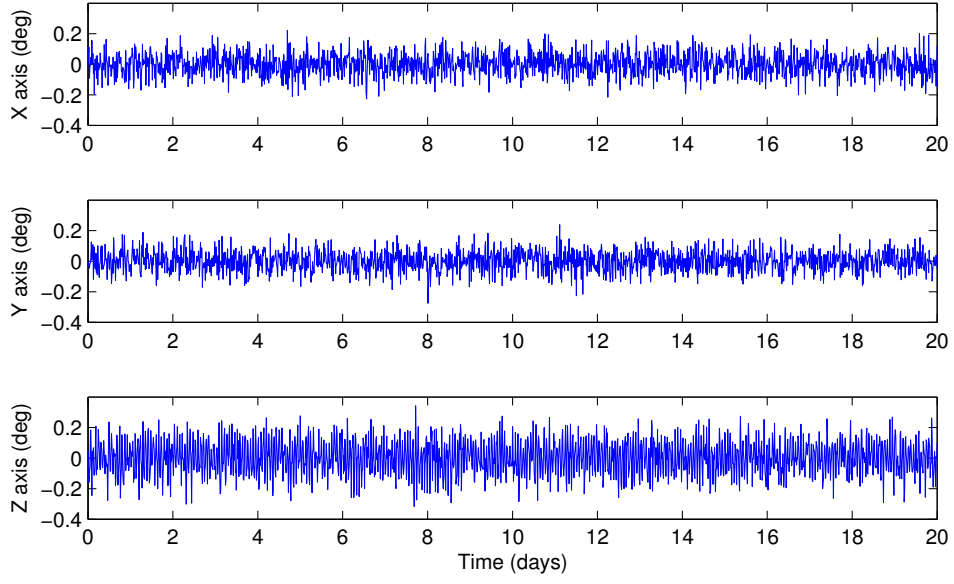


**Fig. 6 Attitude tracking error.**

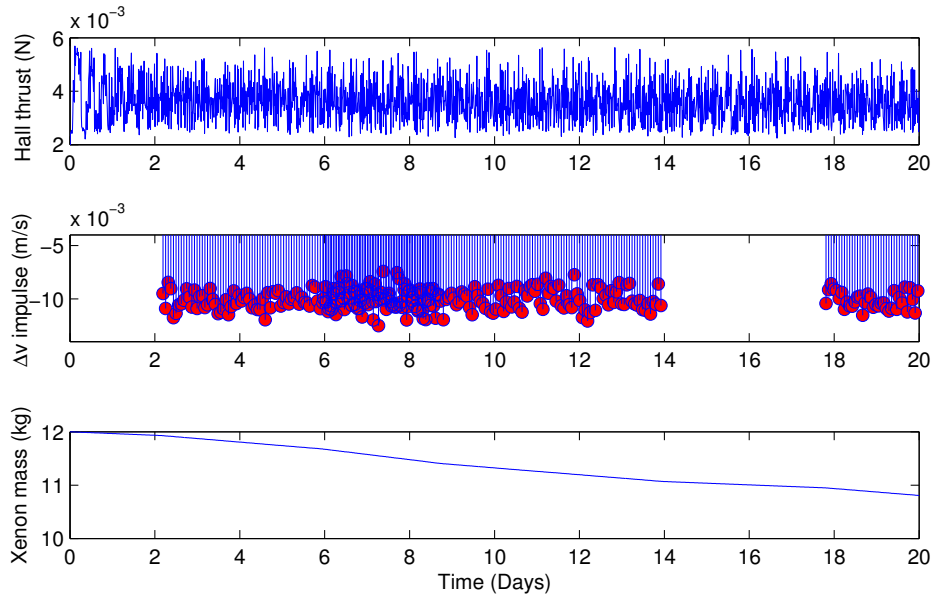


**Fig. 7 Propulsion system performance.**

## VI. Conclusions

The paper has proven that electric propulsion systems can be effective for autonomous station keeping in low Earth orbit missions. The considered Hall effect thruster is able to counteract the

in-track component of atmospheric drag for a sufficiently long mission lifetime. The proposed hybrid continuous/impulsive propulsion scheme permits to compensate also the cross-track perturbations, by using a low power resistojet which is fed by the same propellant tank. This provides a suitable trade-off between thrust efficiency and complexity of the spacecraft internal layout. The simulation results demonstrate the viability of the proposed solution, in terms of both accuracy of the guidance, navigation and control scheme, and performance of the propulsion system. It is believed that this type of technology will play a key role in a number of future low-cost missions for remote sensing and Earth observation.

### References

- [1] Oleson, S. R., Myers, R. M., Kluever, C. A., Riehl, J. P., and Curran, F. M., “Advanced Propulsion for Geostationary Orbit Insertion and North-South Station Keeping,” *Journal of Spacecraft and Rockets*, Vol. 34, No. 1, 1997, pp. 22–28, doi: 10.2514/2.3187.
- [2] Romero, P., Gambi, J. M., Patiño, E., and Antolin, R., “Optimal Station Keeping for Geostationary Satellites with Electric Propulsion Systems Under Eclipse Constraints,” *Progress in Industrial Mathematics at ECMI 2006*, Vol. 12 of *Mathematics in Industry*, Springer-Verlag, Berlin, Germany, 2008, pp. 260–264, doi: 10.1007/978-3-540-71992-2\_31.
- [3] Mailhe, L. M. and Heister, S. D., “Design of a Hybrid Chemical/Electric Propulsion Orbital Transfer Vehicle,” *Journal of Spacecraft and Rockets*, Vol. 39, No. 1, 2002, pp. 131–139, doi: 10.2514/2.3791.
- [4] Manzella, D., “Low Cost Electric Propulsion Thruster for Deep Space Robotic Missions,” *2007 NASA Science Technology Conference*, Hyattsville, Maryland, June 2007, Paper No. 07-0116.
- [5] Patel, P., Scheeres, D., and Gallimore, A., “Maximizing Payload Mass Fractions of Spacecraft for Interplanetary Electric Propulsion Missions,” *Journal of Spacecraft and Rockets*, Vol. 43, No. 4, 2006, pp. 822–827, doi: 10.2514/1.17433.
- [6] Muzi, D. and Allasio, A., “GOCE: The First Core Earth Explorer of ESA’s Earth Observation Programme,” *Acta Astronautica*, Vol. 54, No. 3, 2004, pp. 167–175, doi: 10.1016/S0094-5765(02)00296-5.
- [7] Canuto, E. and Massotti, L., “All-propulsion design of the drag-free and attitude control of the European satellite GOCE,” *Acta Astronautica*, Vol. 64, No. 2-3, 2009, pp. 325 – 344, doi: 10.1016/j.actaastro.2008.07.017.
- [8] Fleck, M. E. and Starin, S. R., “Evaluation of a Drag-free Control Concept for Missions in Low Earth Orbit,” *AIAA Guidance, Navigation, and Control Conference and Exhibit*, Paper No. 03-5747, Austin,

Texas, August 2003.

- [9] Blandino, J., Marchetti, P., and Demetriou, M., “Electric Propulsion and Controller Design for Drag-Free Spacecraft Operation,” *Journal of Spacecraft and Rockets*, Vol. 45, No. 6, 2008, pp. 1303–1315, doi: 10.2514/1.36307.
- [10] Fearn, D., “Economical Remote Sensing from a Low Altitude with Continuous Drag Compensation,” *Acta Astronautica*, Vol. 56, No. 5, 2005, pp. 555–572, doi: 10.1016/j.actaastro.2004.09.052.
- [11] Königsmann, H. J., Collins, J. T., Dawson, S., and Wertz, J. R., “Autonomous Orbit Maintenance System,” *Acta Astronautica*, Vol. 39, No. 9-12, 1996, pp. 977–985, doi: 10.1016/S0094-5765(97)00084-2.
- [12] Boain, R. J., “A-B-Cs of Sun-Synchronous Orbit Mission Design,” *Spaceflight Mechanics 2004*, Vol. 119 of *Advances in the Astronautical Sciences Series*, Univelt, Incorporated, San Diego, California, 2005, pp. 85–104.
- [13] Vallado, D. A., *Fundamental of Astrodynamics and Applications*, Microcosm Press, El Segundo, California, 2nd ed., 2001, Chap. 11.
- [14] De Florio, S. and D’Amico, S., “Optimal Autonomous Orbit Control of a Remote Sensing Spacecraft,” *Spaceflight Mechanics 2009*, Vol. 134 of *Advances in the Astronautical Sciences Series*, Univelt, Incorporated, San Diego, California, 2009, pp. 949–968.
- [15] Polzin, K. A., Markusic, T. E., Stanojev, B. J., DeHoyos, A., Raitses, Y., Smirnov, A., and Fisch, N. J., “Performance of a Low-Power Cylindrical Hall Thruster,” *Journal of Propulsion and Power*, Vol. 23, No. 4, 2007, pp. 886–888, doi: 10.2514/1.28595.
- [16] Loyan, A. V. and Maksymenko, T. A., “Performance Investigation of SPT-20M Low Power Hall Effect Thruster,” *Journal of Technical Physics*, Vol. 49, No. 3-4, 2008, pp. 283–302.
- [17] Nicolini, D., Robertson, D., Chesta, E., Saccoccia, G., Gibbon, D., and Baker, A. M., “Xenon resistojets as a secondary propulsion on EP spacecrafts and performance results of resistojets using Xenon,” *28th International Electric Propulsion Conference*, Toulouse, France, March 2003, Paper No. 03-305.
- [18] Hruby, V., Pote, B., Gamero-Castaño, M., Kolencik, G., Byrne, L., Tedrake, R., and Delichatsios, M., “Hall Thrusters Operating in Pulsed Mode,” *27th International Electric Propulsion Conference*, Pasadena, California, October 2001, Paper No. 01-66.
- [19] Rossetti, P. and Valentian, D., “Analysis of Hall-Effect Thrusters Application to Formation Flying and Drag Compensation,” *30th International Electric Propulsion Conference*, Florence, Italy, September 2007, Paper No. 07-307.
- [20] King-Hele, D., *Satellite orbits in an atmosphere: theory and applications*, Blackie and Son Ltd, London,

- United Kingdom, 1987, Chap. 1.
- [21] Lemoine, F. G., Kenyon, S. C., Factor, J. K., Trimmer, R., Pavlis, N. K., Chinn, D. S., Cox, C. M., Klosko, S. M., Luthcke, S. B., Torrence, M. H., Wang, Y. M., Williamson, R. G., Pavlis, E. C., Rapp, R. H., and Olson, T. R., “The Development of the Joint NASA GSFC and the NIMA Geopotential Model EGM96,” Tech. rep., NASA/TP-1998-206861, 1998.
  - [22] Jacchia, L. G., “Revised Static Models of the Thermosphere and Exosphere with Empirical Temperature Profiles,” Tech. Rep. 332, Smithsonian Astrophysical Observatory, 1971.
  - [23] Wertz, J. R., *Spacecraft attitude determination and control*, Reidel Publishing Company, Dordrecht, Holland, 1978, Chap. 17.
  - [24] Montenbruck, O. and Gill, E., *Satellite Orbits*, Springer-Verlag, Berlin, Germany, 2000, Chap. 3.
  - [25] Barton, C., “International Geomagnetic Reference Field: The Seventh Generation,” *Journal of Geomagnetism and Geoelectricity*, Vol. 49, No. 2-3, 1997, pp. 123–148.
  - [26] Vallado, D. A., *Fundamental of Astrodynamics and Applications*, Microcosm Press, El Segundo, California, 2nd ed., 2001, Chap. 5.
  - [27] Woffinden, D. C. and Geller, D. K., “Relative Angles-Only Navigation and Pose Estimation for Autonomous Orbital Rendezvous,” *Journal of Guidance, Control, and Dynamics*, Vol. 30, No. 5, 2007, pp. 1455–1469, doi: 10.2514/1.28216.
  - [28] Pittelkau, M. E., “Rotation Vector in Attitude Estimation,” *Journal of Guidance, Control, and Dynamics*, Vol. 26, No. 6, 2003, pp. 855–860, doi: 10.2514/2.6929.
  - [29] Crassidis, J. L. and Junkins, J. L., *Optimal Estimation of Dynamic Systems*, Chapman & Hall/CRC press, Boca Raton, Florida, 2004, Chap. 5.
  - [30] Bortz, J. E., “A New Mathematical Formulation for Strapdown Inertial Navigation,” *IEEE Transactions on Aerospace and Electronic Systems*, Vol. 7, No. 1, 1971, pp. 61–66, doi: 10.1109/TAES.1971.310252.
  - [31] Brouwer, D., “Solution of the Problem of Artificial Satellite Theory Without Drag,” *Journal of Guidance, Control, and Dynamics*, Vol. 64, No. 1274, 1959, pp. 378–397.
  - [32] Vallado, D. A., *Fundamental of Astrodynamics and Applications*, Microcosm Press, El Segundo, California, 2nd ed., 2001, Chap. 2.
  - [33] Zeiler, O., Schubert, A., Häusler, B., and Puls, J., “Autonomous Orbit Control for Earth-Observation Satellites,” *4th ESA International Conference on Spacecraft Guidance, Navigation and Control Systems*, Noordwijk, the Netherlands, October 1999, pp. 189–194.
  - [34] Schaub, H., Vadali, S. R., Junkins, J. L., and Alfriend, K. T., “Spacecraft Formation Flying Control Using Mean Orbit Elements,” *Journal of the Astronautical Sciences*, Vol. 48, No. 1, 2000, pp. 69–87.

- [35] Micheau, P., “Orbit control techniques for low Earth orbiting (LEO) satellites,” *Spceflight Dynamics*, Vol. 1, Cépaduès Éditions, Toulouse, France, 1995, pp. 793–902.
- [36] Breger, L. and How, J. P., “Gauss’s Variational Equation-Based Dynamics and Control for Formation Flying Spacecraft,” *Journal of Guidance, Control, and Dynamics*, Vol. 30, No. 2, 2007, pp. 437–448, doi: 10.2514/1.22649.
- [37] Gurfil, P., “Control-Theoretic Analysis of Low-Thrust Orbital Transfer Using Orbital Elements,” *Journal of Guidance, Control, and Dynamics*, Vol. 26, No. 6, 2003, pp. 979–983, doi: 10.2514/2.6926.
- [38] Naasz, B. J., *Classical Element Feedback Control for Spacecraft Orbital Maneuvers*, Master’s thesis, Department of Aerospace and Ocean Engineering, Virginia Polytechnic Institute and State University, 2002, pp. 31-32.
- [39] Schaub, H. and Alfriend, K. T., “Impulsive Feedback Control to Establish Specific Mean Orbit Elements of Spacecraft Formations,” *Journal of Guidance, Control, and Dynamics*, Vol. 24, No. 4, 2001, pp. 739–745.